

# Detachment control in KSTAR with Tungsten divertor

Anchal Gupta<sup>a,\*</sup>, David Eldon<sup>b</sup>, Eunnam Bang<sup>c</sup>, KyuBeen Kwon<sup>a</sup>, Hyungho Lee<sup>c</sup>, Anthony Leonard<sup>b</sup>, Junghoo Hwang<sup>c</sup>, Xueqiao Xu<sup>d</sup>, Menglong Zhao<sup>d</sup>, Ben Zhu<sup>d</sup>

<sup>a</sup>*Oak Ridge Associated Universities, 100 ORAU Way, Oak Ridge, TN 37830, USA*

<sup>b</sup>*General Atomics, 3550 General Atomics Ct, San Diego, CA 92121, USA*

<sup>c</sup>*Korea Institute of Fusion Energy, 169-148 Gwahak-ro, Yuseong-gu, Daejeon 34133, Republic of Korea*

<sup>d</sup>*Lawrence Livermore National Laboratory, PO Box 808, Livermore, CA 94550, USA*

---

## Abstract

We have demonstrated detachment control in KSTAR with the new Tungsten divertor using two different control variables. First variable is the attachment friction calculated from 2-Point Model (2PM) using the ion saturation current density from divertor langmuir probes. Second, we used a prototype neural network surrogate model of UEDGE 2D trained on a set of about 70,000 simulations to provide a realtime estimate of heat flux at the outer divertor. We present the successful detachment control results and discuss future improvements in the control infrastructure and control variables for future burning plasma experiments.

---

## 1. Introduction

Burning plasma tokamaks such as ITER[1], SPARC[2], and the various DEMO concepts are estimated to exhaust very high heat flux in the Scrape-off Layer (SOL) towards the divertor target. As part of the very hot core plasma escapes the magnetic confinement within the last closed flux surface, the hot ions rapidly travel along the open field lines in SOL region towards the divertor targets. To withstand the high heat flux, the divertor target plates are planned to be made out of tungsten which has high strength and the highest melting point of any metal. However, tungsten being a very high-Z material poses contamination challenges for the core plasma and it is important to develop operation strategies that limit the tungsten sputtering, especially in the divertor region where hot plasma interacts with the tungsten surface in a very narrow region of the order of a few mm[3]. Thus, experimental reactors such as KSTAR are in the process of upgrading their divertor and vessel walls to tungsten to design control systems and perform plasma studies in the presence of tungsten contamination.

It is estimated that for steady-state operation, the constant heat flux reaching the divertor plates has to be below 10-15 MW/m<sup>2</sup>[4] to avoid surface melting and structural damage to the divertor plates. Additionally, the electron temperature at the target plate must be below 8 eV[5] to avoid sputtering of tungsten and subsequent contamination of the core plasma. The heat flux reaching the divertor is typically reduced by puffing in gas in the SOL region to dissipate energy and momentum from the exhaust plasma through ionization, charge exchange, and radiation. As the puffed gas neutrals travel toward the core plasma, they radiate energy based on local electron temperature and density. At higher temperatures, more and more electrons get

stripped away from the neutral atoms and the radiation reduces and the main dissipation mechanism becomes charge exchange and ionization. Thus for effective and fast cooling, impurity gases such as nitrogen, neon, and argon are puffed which can dissipate heat through radiation farther away from the divertor. In the presence of such radiative dissipation, the plasma reaching the divertor reduces, effectively reducing the total ion flux which impinges on the divertor. This phenomenon is known as detachment onset as the wetted surface by plasma is reduced. When only part of the surface is wetted, the plasma is said to be partially detached, while if the ion flux is almost completely stopped with higher neutral gas pressure, it is said to be fully detached.

It is important though to keep the amount of impurity gases injected into the vessel to a minimum as higher gas injection eventually leads to more impurity reaching in the pedestal region of the plasma. This can lead to rapid cooling which can collapse H-mode and could also lead to disruption of the plasma confinement. Such sudden loss of plasma confinement can cause damage to the plasma-facing components. Thus, it is important to carefully control the amount of impurity injected to keep the divertor cool while not contaminating the core plasma too much.

There are two key ways to control the heat flux reaching the divertor. The first is to control the radiated power from the SOL region to maintain optimum dissipation of heat before it reaches the divertor. This has been successfully demonstrated in various machines: using the bolometer chords in divertor region in Alcator C-Mod[6], JT-60U[7], ASDEX Upgrade[8] and DIII-D[9], using AXUV diodes in EAST[10], using VUV N VII line emission in JET[11], and using C-III emission radiation front measured using MANTIS in TCV[12].

The second way is to control the degree of plasma detachment from divertor target plates. This has been demonstrated widely in several machines as well: using divertor plate tem-

---

\*Corresponding author

Email address: guptaa@fusion.gat.com (Anchal Gupta)

perature measurements with surface thermocouples in Alcator C-Mod[13], using surface electron temperature measurements with triple-tip Langmuir probes in EAST[14], using ion saturation current measurements from embedded Langmuir probes in JET[15], EAST[16], and DIII-D[14]. In KSTAR, the ion saturation current measurements along with core electron density, injected power, and local magnetic field were used to calculate a derived control variable,  $A_{frac}$ , which was used to control the detachment[17]. This technique has the added benefit that the rollover ion saturation current does not need to be calculated or estimated prior to the shot and thus this technique has the potential for wider applicability in different scenarios and other machines. In this work, we have re-used this technique in our experiments at KSTAR with a tungsten divertor to test the robustness of this control variable in the presence of high-Z contamination from tungsten.

In this work, we have also tested a new technique that uses a machine-learning-based surrogate model, DivControlNN[18]. This model integrates measurements from several realtime inputs to run through a large database of 2D UEDGE[19] simulations and provide a realtime estimate of the heat flux reaching the divertor plates along with several other key plasma parameters upstream in SOL and at the two divertors. We tested a prototype of this model with training and input limitations in KSTAR and demonstrated detachment control for the first time using such a surrogate model. This paves the way for utilizing such models in future reactors that will have a very limited set of sensors available for control systems.

This paper is organized as follows. In Sec.2, we describe the experimental setup and the definition of different control variables used for detachment control. In Sec.3, we describe our experimental shots used for identifying the system and using the fitted plant model to tune a PI controller using frequency response for closed-loop stability analysis and optimization. In Sec.4, we show the results of our detachment control attempts. Finally, in Sec.5, we discuss our results, the possible improvements we can make in the future, and other interesting contemporary work and ideas in the field of detachment control.

## 2. Experimental setup and control variables

The experiment was conducted on a standard single lower null H-mode plasma profile with reference shot KSTAR #35851 with the equilibrium profile as shown in Fig.1. The plasma shaping steps commenced by 7s and the shot was programmed for flat-top up to 17s providing a 10s long window for detachment control experiment. For heat flux control, N<sub>2</sub> gas puffing was used. The heat flux control variable was tested with several different inputs.

First, we utilized previously developed  $A_{frac}$  [17], which is defined as the ratio of measured ion saturation current to modeled (using 2PM[20]) ion saturation current assuming fully attached plasma.  $A_{frac}$  is a convenient choice of control variable that is easily available in most tokamaks and allows for cross-comparison among machines. If the strike point on the diverter tile is fixed in position well enough by the shape control system, a single close-by Langmuir probe is enough to pro-

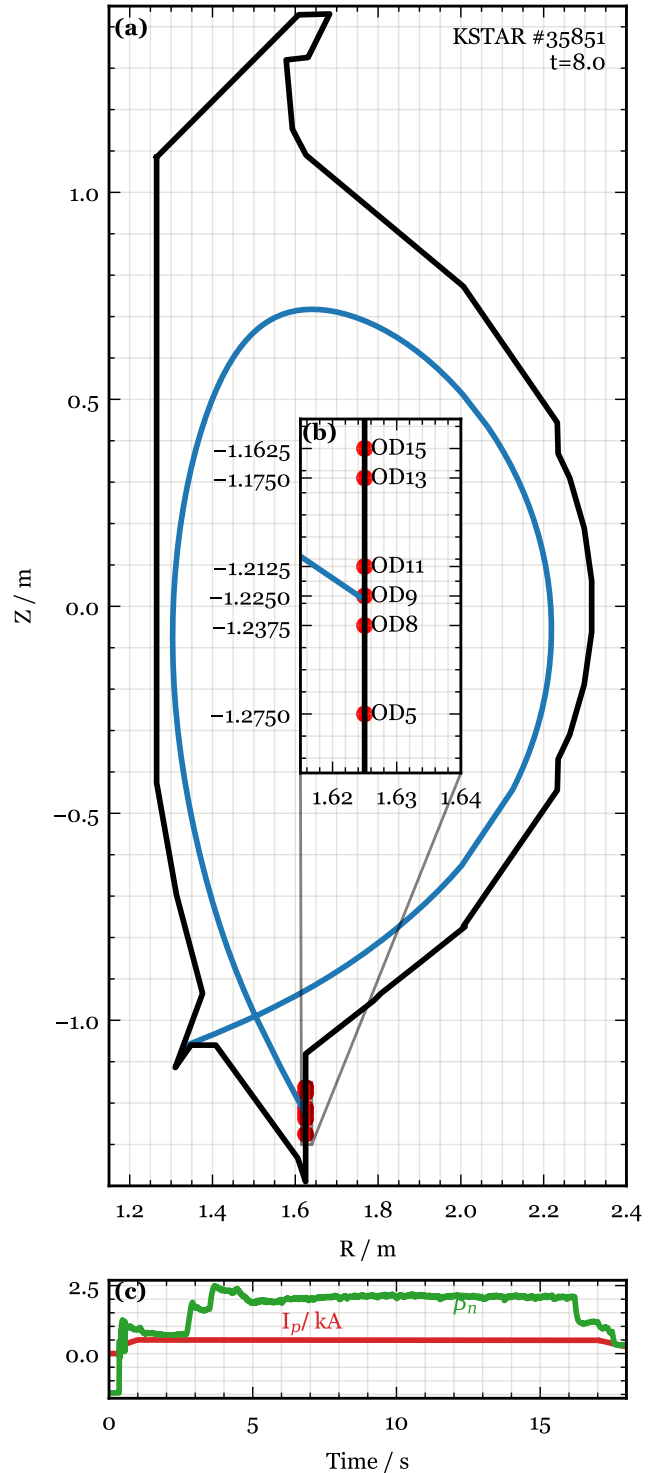


Figure 1: Reference shot #35851. (a) Showing last closed flux surface at t=8 seconds. The magnetic shape control was programmed to keep X point fixed which provided a sufficiently stable strike point on the realtime Langmuir Probe array. (b) Zoomed-in locations of realtime Outer Divertor (OD) Langmuir probes. (c) Plasma current ( $I_p$ ) and  $\beta_n$  for reference shot.

vide the ion saturation current required for  $A_{frac}$  calculation. However, if the strike point control is not good enough, or if it is required to leave it as a free variable to allow for control-

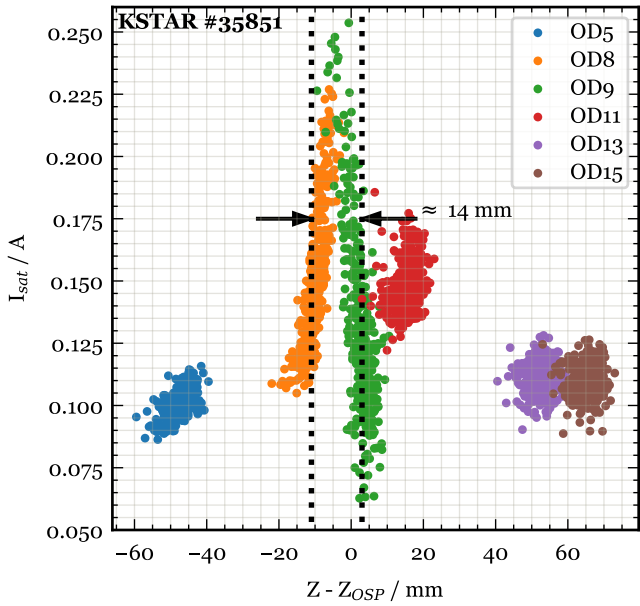


Figure 2: Strike point width estimation for reference shot #35851. The raw data from Langmuir probe array has been filtered by 8th order Butterworth filter with cut-off frequency of 20 Hz and then down sampled to 40 Hz. For each data point on this plot, the x-axis position is calculated by subtracting the outer strike point (OSP) position reported by EFIT from the probe's Z coordinate. The black dotted lines represent the rough estimate for width of strike point ion saturation current profile taken at half the maximum value above baseline.

ling other parameters in the shape control loop (as was the case in our experiments), then it is required to estimate the true ion saturation current through measurements made by a Langmuir probe array. In our experiments, we chose the peak value from the Langmuir probe array as the input to the ion saturation current at the strike point. Fig. 2 plots the data from this Langmuir probe array for our reference shot. The horizontal axis in this figure has been referenced from the EFIT reported outer strike point (OSP) position. Thus, this figure shows the spread of the ion saturation current profile across the strike point. Here, we see that the strike point is closer to OD8 and OD9 with a peak ion saturation current value of roughly 0.25 A at the strike point position. We estimate the width of the ion saturation current profile at half the maximum value referenced to the baseline value of 0.1 A measured by far away probes, giving approximately at least a 14 mm wide profile. This ensures that the Langmuir probe array as shown in Fig. 1 would always have at least one probe that can confidently measure the ion saturation current for the strike point when the strike point is within the closely placed probes, OD8, OD9, and OD11.

Langmuir probes would not be able to survive high heat flux in burning plasma future reactors. In general, such reactors would be severely limited in the number of realtime sensors available for control systems because of high neutron fluence and heat flux in vacuum vessels, and thus alternate control variables need to be searched for. Toward this goal, we tested a prototype of a machine-learning-based surrogate model of 2D UEDGE, DivControlNN. The employed version of DivCon-

trolNN is trained on approximately 70,000 2D UEDGE simulations of KSTAR. The training dataset scanned core electron density ( $1.5 \times 10^{19} - 7.0 \times 10^{19} \text{ m}^{-3}$ ), plasma current (600 – 800 kA), injected total power through NBI and ECH (1 – 8 MW), impurity fraction with respect to Deuterium density (0 – 0.04), and scaling of diffusion coefficient profile with a factor (0.6 – 2). The diffusion coefficient profile is assumed for a typical H-mode shot which can be scaled as an input to the model. This provided a widely applicable surrogate model that gives steady-state values of heat flux, ion saturation current, and electron temperature along the two divertors, electron density and temperature at the upstream point of the midplane, and total radiated power, power fraction radiated from divertor, and peak radiation power location in the poloidal cross-section of the device. The model generates output within 20% error from the 2D UEDGE output.

DivControlNN was originally developed and trained using Python's TensorFlow package and consists of two different models working in tandem. The first is a multi-modal  $\beta$ -variational autoencoder[21] model to compress various quantities of interest coming from synthetic diagnostics on a 2D UEDGE database into a latent space representation. The second stage is a multi-layer perceptron (MLP) model that maps the inputs of the 2D UEDGE simulations (which also form the inputs to the overall surrogate model). During inference operation, the MLP model first maps the inputs to the latent space and the decoder network from the autoencoder then decodes the latent space into useful outputs. While Python is the industry choice for developing and training such models, it can not be used for real-time inference purposes such as our use case. We converted the Python model into a pure C code using a keras2c[22] package which is developed for generally converting such neural networks into real-time compatible C codes. The generated C code runs an inference operation in about 160  $\mu\text{s}$  on Intel® Core™ i7-6600U CPU @ 2.60GHz while we saw speed up of upto 18  $\mu\text{s}$  per inference on Apple® M2™ Pro. The real-time PCS in KSTAR runs its divertor control categories in a 5  $\mu\text{s}$  clock cycle CPU, so we ran DivControlNN in a separate 1 ms clock-cycle CPU ensuring enough runtime for it along with other processes in that CPU. This was still more than sufficient for our control purposes which anyway can not control faster than a few 10s of Hz due to system response time and gas actuation speed.

This preliminary model, however, has been trained on 2D UEDGE simulations of KSTAR with carbon divertor and carbon as the sole impurity species. So it does not reflect the same Tungsten divertor system in which it was tested. There were several other limitations to the realtime input provided to the model. There was no reliable input for impurity fraction in plasma and we created an ad-hoc gas accumulation model which estimated impurity fraction by taking the ratio of total puffed impurity with total puffed Deuterium gas with estimated decay rates to model the effect of pumping and wall adsorption. Additionally at KSTAR, the total input power from NBI and ECH sources is not completely available in realtime PCS and we had to input a feedforward signal matching the programmed rate of some sources that got summed with the other sources whose power was available in realtime. Finally, the diffusion

coefficient scaling factor was set to 1.0 for lack of any better realtime information on it. Despite these limitations, we attempted to use this model as a preliminary test for using such a surrogate model in real time and identify major obstacles before testing an improved and more relevant version in the future.

### 3. System identification and Controller Tuning

Before we attempted detachment control experiments, we took two system identification shots. The data from the first system identification shot #35853 is shown in Fig.3. In this shot, we puffed in N<sub>2</sub> gas in steps of 1.0 V, 2.5V, and 4.0 V with puff duration of 1.5s each. A corresponding response was seen in A<sub>frac</sub> but with a delay. We later confirmed from post-shot EFIT data that the strike point was indeed within the realtime Langmuir Probe array and thus our A<sub>frac</sub> calculation was valid. We fitted the measured data with a simple first-order plant model of gain K, time constant  $\tau$ , and time delay L given by:

$$G(s) = \frac{K}{\tau s + 1} e^{-Ls} \quad (1)$$

The fit resulted in an identified model with K = -0.275 ± 0.002,  $\tau = 1.00 \pm 0.02$ s, and L = 0.154 ± 0.006s. The fit is shown in Fig.3b. Note that only the part of the time series data that was used in fit is shown for the fitted curve. This fit was performed in the inter-shot interval during the experiment and has not been improved or modified after the experiment.

The controller gains were chosen by visualizing closed loop transfer function (CLTF) of the system with chosen PI gains as shown in Fig.4. Here, the frequency domain response of the plant model ( $G(s)$ ) and PI controller ( $T_{PI}(s)$ ) are plotted together. When connected in series, this forms the open loop transfer function (OLTF) of the system ( $O(s) = G(s)T_{PI}(s)$ ). The frequency where OLTF becomes 1.0 is called unity gain frequency (UGF). Phase margin is defined as the additional phase delay at UGF that would make the system unstable by taking it to -180°. Additionally, we also define delay margin as the additional actuation delay that would make UGF unstable. The CLTF is then calculated by solving the loop algebra in the Laplace domain:

$$C(s) = \frac{G(s)}{1 + O(s)} \quad (2)$$

Because of the long delay, we chose to not use a derivative gain. The goal of tuning was to push UGF as high as possible (0.59 Hz) while keeping a reasonable phase margin (14.8 °) and margin for any additional actuation delay (69 ms). This resulted in controller settings as: K<sub>p</sub> = -10.0, T<sub>i</sub> = 253.0 ms, and  $\tau_s$  = 50.0 ms, where K<sub>p</sub> is proportional gain, T<sub>i</sub> is integral time, and  $\tau_s$  is pre-smoothing time constant. This is still a very aggressive choice of controller, but provided that the system identification fit gave an unexpectedly high value of response time  $\tau = 1$ s probably due to too much noise during small step inputs, we decided to go ahead with this controller choice. The resulting PI controller transfer function is given by:

$$T_{PI}(s) = K_p \left( \frac{1}{T_i s} + 1 \right) \frac{1}{1 + \tau_s s} \quad (3)$$

Unfortunately, the surrogate model was not configured properly in this system identification shot due to technical errors, so we repeated a system identification but this time we decided to keep the nitrogen valve in the constant open position, to look for any deviation in the behavior. The data from this second system identification shot is shown in Fig.5. Despite all the limitations of DivControlNN as listed earlier, we still saw a good correlation in the DivControlNN heat flux output at the outer divertor with the injected gas as seen in Fig.5b. This is validated by estimated A<sub>frac</sub> in Fig.5d showing an increase in detachment level as the predicted output heat flux decreases. The strike point was maintained within the realtime Langmuir probe array (Fig.5a) validating the output of A<sub>frac</sub>. Note that we have not yet calibrated the DivControlNN model with any experimental data, so we treated the output as arbitrary units and later attempted to control the detachment with estimated changes to this arbitrary output.

We again fitted this system with a first-order system with delay as described in Eq.1. The fit resulted in an identified model with K = -0.302 ± 0.004,  $\tau = 0.31 \pm 0.03$ s, and L = 0.536 ± 0.019s. The fit is shown in Fig.5b. Here as well, the fitting shown was performed during the experiment in the inter-shot interval and has not been modified or optimized later. The time domain in which the fitting curve is shown is the data where the system was fitted. Admittedly, this fit was not very good and we did not believe the large lag value to be accurate. So for the purpose of tuning the controller, we arbitrarily set the system lag value to 100 ms. The controller gains were chosen by visualizing CLTF of the system with chosen PI gains as shown in Fig.6 and following the same procedure as we described for A<sub>frac</sub> controller tuning. The resulting controller settings were: K<sub>p</sub> = -3.0, T<sub>i</sub> = 68.5 ms, and  $\tau_s$  = 5.0 ms creating controller given by Eq.3. Here, we estimated to achieve a UGF of 1.01 Hz, phase margin of 11.9 °, and delay margin of 33 ms. This controller was also very aggressive, but we decided to go ahead with this controller choice given the limitations of the system identification fit and lack of time for further analysis in between the allotted run time of our experiment.

## 4. Results

Utilizing the controllers tuned in Sec.3, we attempted detachment control experiments. First, we used A<sub>frac</sub> controller in KSTAR #35857 with results shown in Fig.7. As can be seen in Fig.7a, the strike point remained within the realtime Langmuir probe array giving validity to the A<sub>frac</sub> signal shown in Fig.7b. Here, we can see that the controller was successful in closely following the target provided to it completing the pre-programmed shot length to the end. It is also evident that the aggressive control strategy was good and did not result in any long sustained oscillations while providing a quick response to the changing target value. From 8s to 10s, it can be seen that the injected N<sub>2</sub> was just enough to ramp down the measured

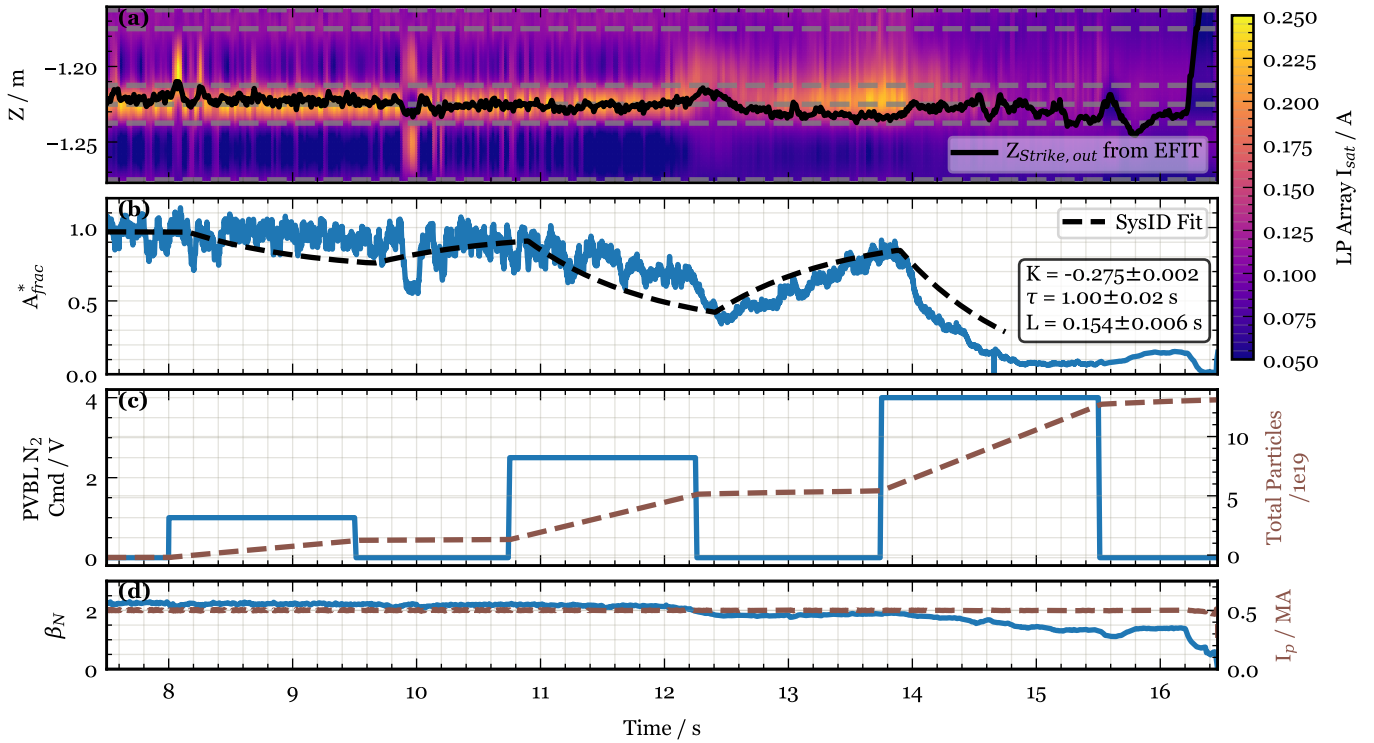


Figure 3: System identification shot #35853. (a) Shows the measured ion saturation current by realtime Langmuir Probe array at locations marked by grey dashed lines. The data has been interpolated spatially using cubic spline interpolation. The black curve shows the post-shot calculated strike point position on outer divertor using EFIT. (b) Shows the  $A_{frac}$  calculated from peak value among the Langmuir probe array. The dashed black line shows the system identification fit on this data. (c) Left axis: Shows the  $N_2$  gas command steps sent for system identification. Right axis: Shows the cummulative  $N_2$  gas particles injected into the vessel. (d) Left axis: Shows  $\beta_N$ . Right axis: Shows the plasma current ( $I_p$ ). \* Note:  $A_{frac}$  for this shot was not calibrated properly and the raw data reported 2 times the value. We fixed this factor after this shot and this figure shows the corrected value.

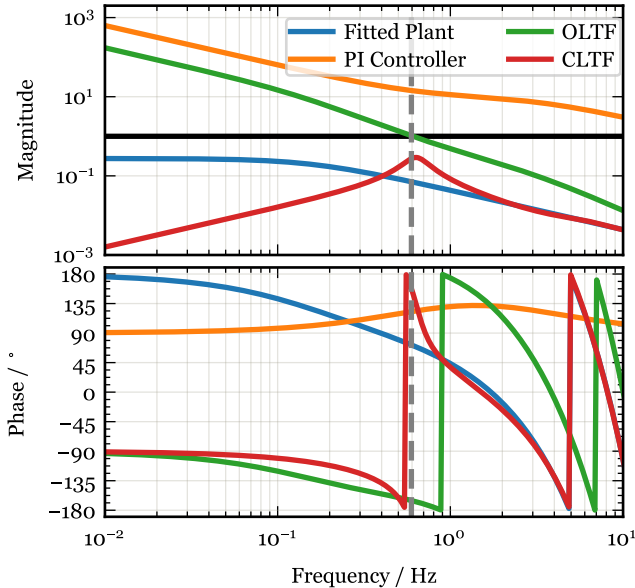


Figure 4: Closed loop transfer function analysis of the system using  $A_{frac}$  output with chosen PI controller with gains:  $K_p = -10.0$ ,  $T_i = 253.0$  ms, and  $\tau_s = 50.0$  ms. The dashed grey verticle line shows the unity gain frequency (UGF) of the system.

$A_{frac}$  with the same slope. The accumulated offset from the target eventually caused the integral term to send a brief impulse of nitrogen near 9.8s and then the controller further converged with the target value. For the rest of the shot, small nitrogen puffs were required to correct the drifting  $A_{frac}$  and keep it on the target. The total radiated power from the plasma as measured by KSTAR Infra-Red Video Bolometer (IRVB) remained below 3.5 MW and as can be seen in Fig. 9a (snapshot taken at around the time of maximum radiation), the majority of the radiation was coming from the divertor region and the core region was not loosing power through radiation. This further validated, that  $A_{frac}$  controller strategy first devised in Ref.[17] is a viable option for detachment control even with Tungsten divertor in KSTAR.

Since  $A_{frac}$  controller has been demonstrated in the past as well, we decided to utilize the remaining allotted runtime on KSTAR to test the DivControlNN prototype-based controller. Fig. 8 shows the results from shot #36161 where we deployed this controller. An immediate issue was seen with DivControlNN output that the initial heat flux calculation had a different starting value than what we saw in reference shots and system identification shot #35854. Because of this, when the controller turned on at 7.5s, the large error resulted in the railing of gas command output which caused too much  $N_2$  injected into the system. While this quickly brought down the measured

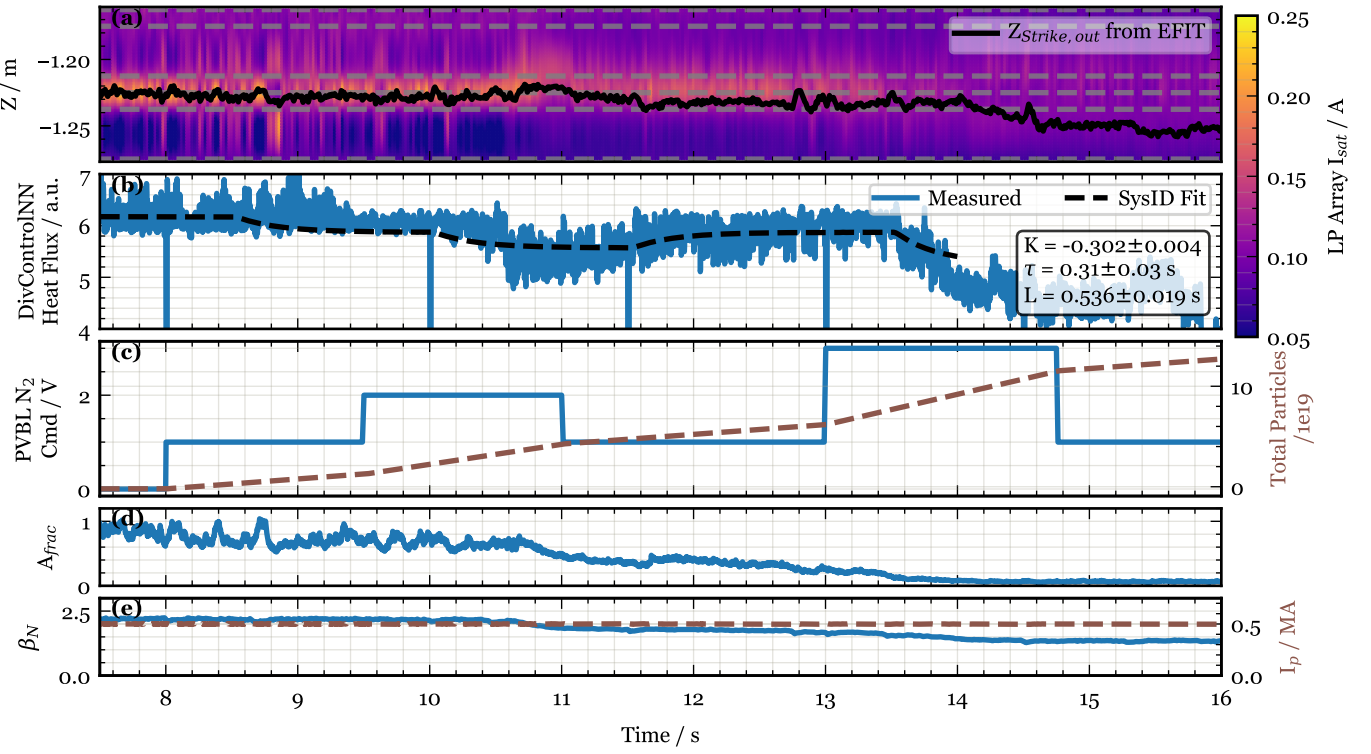


Figure 5: System identification shot #35854. (a) Shows the measured ion saturation current by realtime Langmuir Probe array at locations marked by grey dashed lines. The data has been interpolated spatially using cubic spline interpolation. The black curve shows the post-shot calculated strike point position on outer divertor using EFIT. (b) Shows the heat flux at outer divertor calculated by DivControlNN. The dashed black line shows the system identification fit on this data. (c) Left axis: Shows the N<sub>2</sub> gas command steps sent for system identification. Right axis: Shows the cummulative N<sub>2</sub> gas particles injected into the vessel. (d) Shows the A<sub>frac</sub> calculated from peak value among the Langmuir probe array. (e) Left axis: Shows  $\beta_N$ . Right axis: Shows the plasma current ( $I_p$ ).

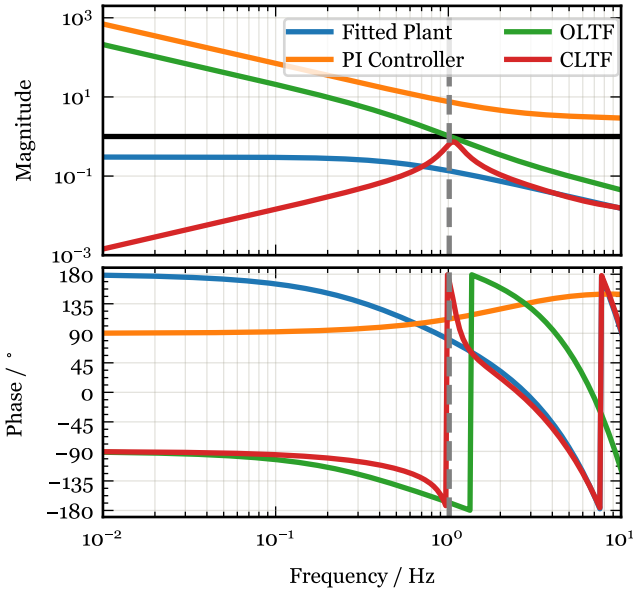


Figure 6: Closed loop transfer function analysis of the system using DivControlNN heat flux at outer divertor output with chosen PI controller with gains:  $K_p = -3.0$ ,  $T_i = 68.5$  ms, and  $\tau_s = 5.0$  ms. The dashed grey verticle line shows the unity gain frequency (UGF) of the system.

signal, it also resulted in an overshoot. In the next ramp-down of the target from 10.5s to 11.5s, more impurity was injected as we tuned an aggressive controller. It can be seen from  $A_{frac}$  in Fig.8d that the system reached deep detachment by this point and the ion saturation current measurements (Fig.8a) became unreliable beyond 11s. In post-analysis of IRVB inverted data as shown in Fig.9, we can see that the core started radiating a lot of power after the last railed impulse of gas input between 10.8s to 12s. This perhaps caused enough cooling of the core and the cross-drift of power into SOL region reduced. This might be why the heat flux (Fig.8b) did not naturally recover even when the target was lifted between 13s to 15s. There is no surprise with the fact that setting target values for an uncalibrated output is not always deterministic and would cause issues as we faced.

Post-shot data analysis discovered further issues in our operation of the DivControlNN model. The impurity fraction calculation as mentioned in 2 malfunctioned and sent a constant zero input to the model. Thus the model was unable to respond to large amounts of impurity that were injected into the system and was only relying on data from line-integrated core electron density and plasma current as realtime inputs. In the past it has been seen that deuterium alone is sufficient to attain partial detachment[23, 24]. This might be the case with shot #36161, that the model inference with zero impurity fraction input still reported a decrease in estimated heatflux as the electron density

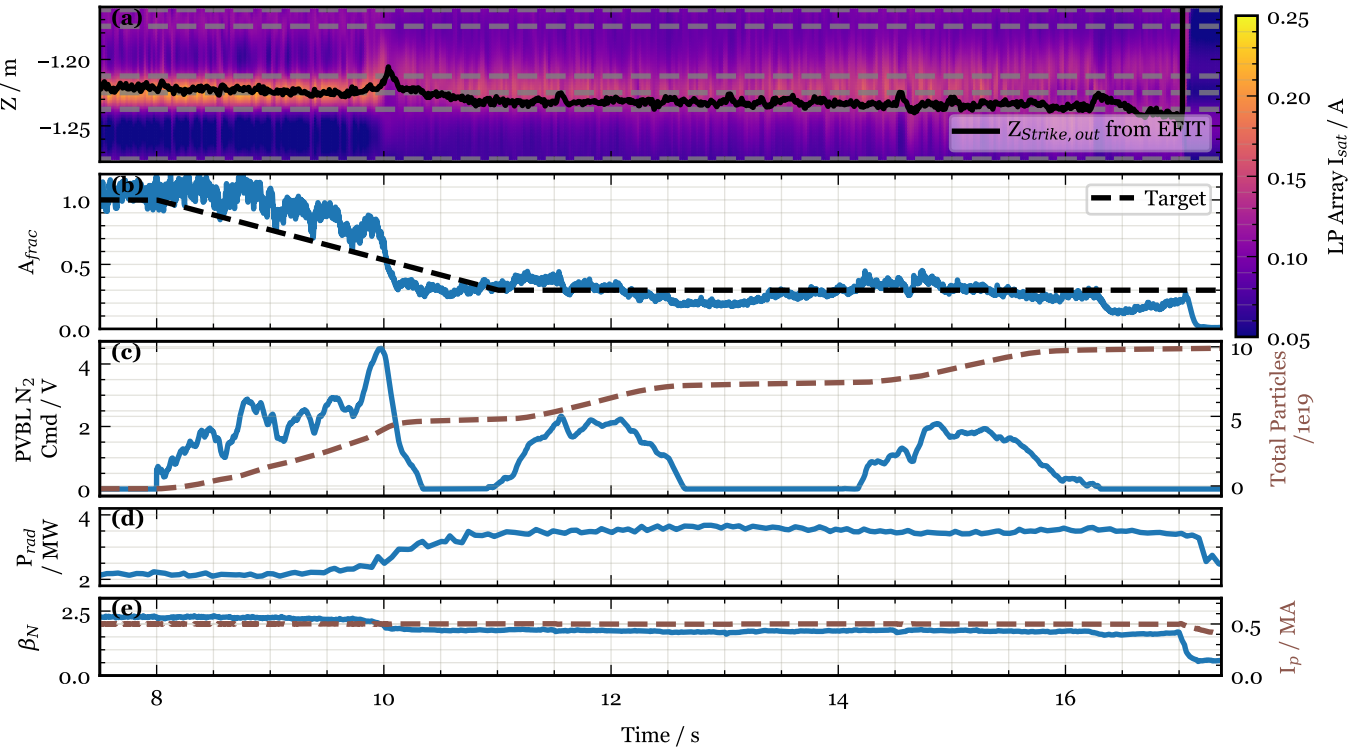


Figure 7: Detachment control shot #35857 using  $A_{frac}$  controller. (a) Shows the measured ion saturation current by realtime Langmuir Probe array at locations marked by grey dashed lines. The data has been interpolated spatially using cubic spline interpolation. The black curve shows the post-shot calculated strike point position on outer divertor using EFIT. (b) Shows the  $A_{frac}$  calculated from peak value among the Langmuir probe array. The dashed black line shows the target provided to the controller to follow. (c) Left axis: Shows the  $N_2$  gas command steps sent for system identification. Right axis: Shows the cummulative  $N_2$  gas particles injected into the vessel. (d) Total radiated power measured by Infra-Red Video Bolometer (IRVB). (e) Left axis: Shows  $\beta_n$ . Right axis: Shows the plasma current ( $I_p$ ).

input increased with  $N_2$  puffing. The only other changeable input, input power, mostly remained constant during flat top of the shot. However, as the amount of total puffed  $N_2$  increased, the pure deuterium plasma case from which the model must be inferring the heat flux would deviate and thus the control is not very good beyond 11s. Despite these limitations, this preliminary test sheds light on the potential of using such a surrogate model-based controller for detachment control in future reactors.

## 5. Discussion

In this paper, we described re-using  $A_{frac}$  as a reliable control variable for detachment control provided that realtime ion saturation current measurements are available from the Langmuir probes and the strike point is controlled well enough that such an array can be used to calculate  $A_{frac}$ . It can be seen from panels (a) and (c) in Fig.3, Fig.5, and Fig.8 that when the total injected impurity amount crosses a rough threshold of about  $1 \times 10^{20}$  particles, the plasma shape starts to rotate such that strike point on outer divertor starts drifting downwards (and the inner strike point moves upwards) even though the X-point is held in place by the magnetic shape control system. Thus,  $A_{frac}$  controller is best suited with an outer strike point control system commissioned on the device which was not the case for

the KSTAR experimental campaign in which we tested these controllers. It is also important to keep note of the width of the strike point and its profile on the divertor. In our case, we estimated that the strike point width is about 14 mm, just enough to ensure that at least one of the Langmuir probes is always inside the wetted area from the SOL plasma. Even then, it can be seen at around 12.4s in Fig.3 and at around 10s in Fig.7 that as the strike point moves from OD9 ( $Z=-1.225\text{m}$ ) to OD11( $Z=-1.2125\text{m}$ ), the corresponding  $A_{frac}$  value shows a sharp decline and then recovery, probably due to the peak passing through the middle of the two probes. This effect is small enough that our existing controller was able to fix it, but it shows a potential source of error in system identification and might also cause loss of control if the sudden transition can excite an unstable oscillation of the UGF. For future applications of this controller, we are working on including realtime spatial analysis of the strike point profile, potentially informed with profile shapes from high-fidelity simulations from SOLPS-ITER or UEDGE.

It should be noted that in the application of  $A_{frac}$  controller method on KSTAR, tuning the overall factor to  $A_{frac}$  so that it reports 1.0 when fully attached was trickier than the case for full carbon environment KSTAR[17]. We noticed offsets in the outputs of Langmuir probes which changed from shot to shot, and thus ensuring the correct normalizing factor for  $A_{frac}$  became harder. This was the reason why we had to change the

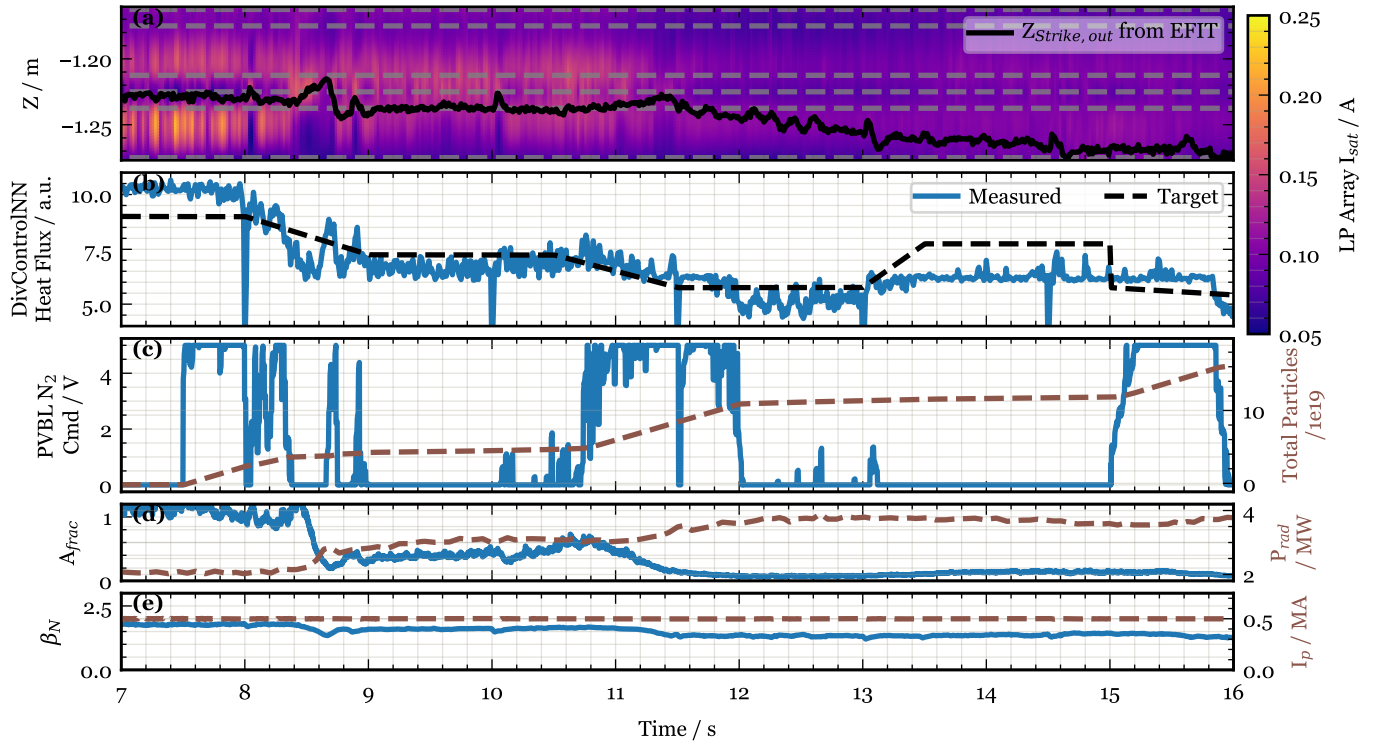


Figure 8: Detachment control shot #36161 using DivControlNN heat flux at outer divertor. (a) Shows the measured ion saturation current by realtime Langmuir Probe array at locations marked by grey dashed lines. The data has been interpolated spatially using cubic spline interpolation. The black curve shows the post-shot calculated strike point position on outer divertor using EFIT. (b) Shows the heat flux at outer divertor calculated by DivControlNN. The dashed black line shows the target provided to the controller to follow. (c) Left axis: Shows the  $N_2$  gas command steps sent for system identification. Right axis: Shows the cummulative  $N_2$  gas particles injected into the vessel. (d) Left axis: Shows the  $A_{frac}$  calculated from peak value among the Langmuir probe array. Right axis: Total radiated power measured by Infra-Red Video Bolometer (IRVB). (e) Left axis: Shows  $\beta_n$ . Right axis: Shows the plasma current ( $I_p$ ).

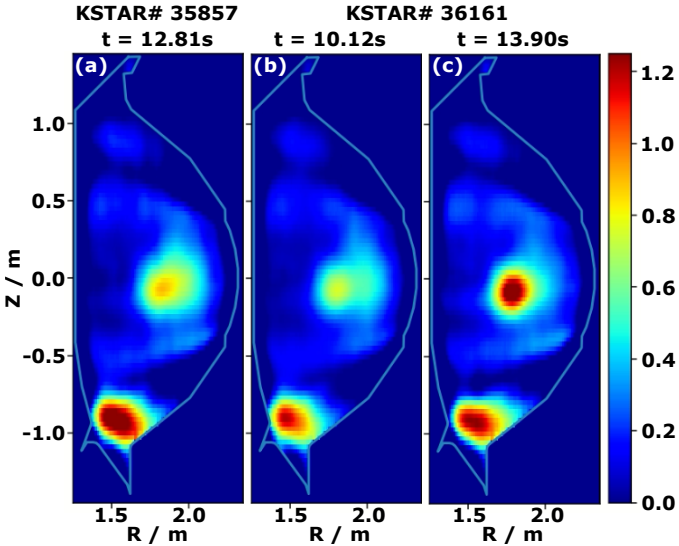


Figure 9: KSTAR Infra-Red Video Bolometer (IRVB) measured radiated power density (a.u.) inverted into 2D cross-section. (a) KSTAR #35857 at 12.81s at the peak of total radiated power. (b) KSTAR #36161 at 10.12s before the second impulse of gas between 10.8s to 12s. (c) KSTAR #36161 at 13.90s after the last gas impulse.

factor for  $A_{frac}$  after shot #35853 as also mentioned in the cap-

tion of Fig.3. After this experience, we have now added an online offset estimator and subtraction for all probe signals, which measures the offset before the plasma breakdown and ensures that the zero offset is correct on the probes. This issue is likely due to electrical connectivity problems with the probes which also showed other issues during the campaign, but still, this experience should be noted for future reproduction and improvements.

Although Langmuir probes might not be able to survive future burning plasma experiments, they are still a valuable tool for studying detachment control experiments for ease of installation and operation in experimental devices. Even in burning plasma devices, sacrificial Langmuir probes can be used in commissioning controllers based on other control variables given the success and reliability of using these probes for detachment control demonstrated on various devices [14, 15, 16]. The good results from  $A_{frac}$  controller as seen in Fig.7 could also motivate further research in similar biased electrode measurement methods of SOL plasma such as biased divertor plates [25, 26] which behave like larger area Langmuir probes and can withstand harsher conditions in comparison to small tip area probes.

We also demonstrated using a machine-learning-based surrogate model, DivControlNN, which infers from a large database of 2D UEDGE simulations for estimating inaccessible quanti-

ties in the plasma, such as heat flux on the divertor, for controlling detachment level with realtime feedback. As of the writing of this manuscript, this detachment control method is the first of its kind ever implemented and will act as a stepping stone for future deployments. This is an important step in the direction of achieving detachment control in future burning plasma reactors which would have very limited means of measuring the detachment level due to space constraints and harsh environment. We have identified critical weak points in the prototype of DivControlNN and the control infrastructure required to utilize this model, and we are working on improving these aspects for future tests. We are in the process of creating a new 2D UEDGE database of KSTAR with a tungsten divertor and considering multiple charged states of additional impurities such as nitrogen, neon, and argon. New models would be trained on the expanded database and acquired experimental data from this campaign, with the input of injected gas flow instead of impurity fraction to simplify the use case of these models. We would also work with the KSTAR team to improve PCS communication infrastructure so that accurate realtime values of injected power are available to our models.

The initial success of the neural network surrogate model in detachment control motivates and corroborates similar studies, simulations, and training of other models for providing fast estimates of plasma parameters, for quick decision-making in the control room during experiments, as well as, for potential use in other control systems where important plasma properties are often not accessible directly. A neural network based control system approach has already been demonstrated in magnetic shape control[27]. For SOL plasma predictions, machine learning surrogate models were first pioneered using 1D UEDGE simulations[28], serving as the proof-of-principle study for the DivControlNN presented here. More recently, model based on Hermes-3[29] simulations of MAST-U[30] and neural partial differential equation solver for TCV[31] have been reported and are under further development.

Another major focus of future experiments would be to use noble gases in detachment control as N<sub>2</sub> while being optimum in cooling the SOL plasma is not allowed in burning plasma devices due to the formation of tritiated ammonia that poses radioactive dangers. We are in the process of testing Ne and Ar as alternate cooling gases. In the medium-sized tokamaks such as KSTAR though, the effect of Ne has been hard to observe as small gas puffs do not actuate enough on the SOL plasma but if the gas puffing is increased, we suddenly observe disruption due to too much cooling inside the separatrix. More widely, there has been recent interest in using pellets for impurity injection for detachment control to reduce the large lag time and response time associated with gas puffing. Another alternative is dropping the impurity in the form of solid powder, such as Boron. However, the investigation on its use for this purpose is still in a preliminary phase and poses additional challenges in terms of long lag time due to free fall and accumulation of unused powder in the device.

## CRediT authorship contribution statement

**A. Gupta** investigation, methodology, software, formal analysis, visualization, writing - original draft. **D. Eldon** conceptualization, software, investigation, writing - review & editing, supervision, funding acquisition. **E. Bang** resources, data curation. **K. Kwon** resources, investigation. **H. Lee** resources, supervision. **A. Leonard** writing - review & editing. **J. Hwang** resources, data curation. **X. Xu** conceptualization, supervision, funding acquisition. **M. Zhao** methodology, software. **B. Zhu** methodology, software

## Declaration of competing interest

The authors declare that they have no known competing financial interests or personal relationships that could have appeared to influence the work reported in this paper.

## Acknowledgements

This material is based upon work supported by the U.S. Department of Energy, Office of Science, Office of Fusion Energy Sciences, under Awards DE-SC002340, and DE-AC52-07NA27344.

## Disclaimer

This report was prepared as an account of work sponsored by an agency of the United States Government. Neither the United States Government nor any agency thereof, nor any of their employees, makes any warranty, express or implied, or assumes any legal liability or responsibility for the accuracy, completeness, or usefulness of any information, apparatus, product, or process disclosed, or represents that its use would not infringe privately owned rights. Reference herein to any specific commercial product, process, or service by trade name, trademark, manufacturer, or otherwise, does not necessarily constitute or imply its endorsement, recommendation, or favoring by the United States Government or any agency thereof. The views and opinions of authors expressed herein do not necessarily state or reflect those of the United States Government or any agency thereof.

## References

- [1] N. Holtkamp, [An overview of the iter project](#), Fusion Engineering and Design 82 (5) (2007) 427–434, proceedings of the 24th Symposium on Fusion Technology.
- [2] A. J. Creely, et al., [Overview of the sparc tokamak](#), Journal of Plasma Physics 86 (5) (2020) 865860502.
- [3] T. Eich, et al., [Scaling of the tokamak near the scrape-off layer h-mode power width and implications for iter](#), Nuclear Fusion 53 (9) (2013) 093031.
- [4] R. Pitts, et al., [Physics basis for the first iter tungsten divertor](#), Nuclear Materials and Energy 20 (2019) 100696.

- [5] S. Brezinsek, et al., [Erosion, screening, and migration of tungsten in the jet divertor](#), Nuclear Fusion 59 (9) (2019) 096035.
- [6] J. A. Goetz, et al., [High confinement dissipative divertor operation on alcator c-mod](#), Physics of Plasmas 6 (5) (1999) 1899–1906.
- [7] N. Asakura, et al., [Investigations of impurity seeding and radiation control for long-pulse and high-density h-mode plasmas in jt-60u](#), Nuclear Fusion 49 (11) (2009) 115010.
- [8] A. Kallenbach, et al., [Optimized tokamak power exhaust with double radiative feedback in ASDEX Upgrade](#), Nucl. Fusion 52 (2012) 122003.
- [9] D. Eldon, et al., [Advances in radiated power control at diii-d](#), Nuclear Materials and Energy 18 (2019) 285–290.
- [10] K. Wu, et al., [Achievement of radiative feedback control for long-pulse operation on east](#), Nuclear Fusion 58 (5) (2018) 056019.
- [11] G. Maddison, et al., [Demonstration of real-time control of impurity seeding plus outboard strike-point sweeping in jet elmy h-mode plasmas](#), Nuclear Fusion 51 (8) (2011) 082001.
- [12] T. Ravensbergen, et al., [Real-time feedback control of the impurity emission front in tokamak divertor plasmas](#), Nature Communications 12 (2021) 1105.
- [13] D. Brunner, et al., [Surface heat flux feedback controlled impurity seeding experiments with alcator c-mod's high-z vertical target plate divertor: performance, limitations and implications for fusion power reactors](#), Nuclear Fusion 57 (8) (2017) 086030.
- [14] D. Eldon, et al., [An analysis of controlled detachment by seeding various impurity species in high performance scenarios on diii-d and east](#), Nuclear Materials and Energy 27 (2021) 100963.
- [15] C. Guillemaut, et al., [Real-time control of divertor detachment in h-mode with impurity seeding using langmuir probe feedback in jet-iter-like wall](#), Plasma Physics and Controlled Fusion 59 (4) (2017) 045001.
- [16] Q. Yuan, et al., [The first implementation of active detachment feedback control in east pcs](#), Fusion Engineering and Design 154 (2020) 111557.
- [17] D. Eldon, et al., [Enhancement of detachment control with simplified real-time modelling on the KSTAR tokamak](#), Plasma Physics and Controlled Fusion 64 (7) (2022) 075002.
- [18] B. Zhu, et al., [Latent space mapping: Revolutionizing predictive models for divertor plasma detachment control](#), Physics of Plasmas (under review).
- [19] T. D. Rognlien, et al., [Two-dimensional electric fields and drifts near the magnetic separatrix in divertor tokamaks](#), Physics of Plasmas 6 (5) (1999) 1851–1857.
- [20] A. W. Leonard, [Plasma detachment in divertor tokamaks](#), Plasma Physics and Controlled Fusion 60 (4) (2018) 044001.
- [21] I. Higgins, et al., [beta-VAE: Learning basic visual concepts with a constrained variational framework](#), in: International Conference on Learning Representations, 2017.
- [22] R. Conlin, A. Gupta, [keras2c \(forked from plasmacontrol/keras2c\). general python keras model to real-time c converter.](#), in: Github with GNU Lesser GPL 3 License, 2024.
- [23] A. Loarte, et al., [Plasma detachment in jet mark i divertor experiments](#), Nuclear Fusion 38 (3) (1998) 331.
- [24] D. Eldon, et al., [Controlling marginally detached divertor plasmas](#), Nuclear Fusion 57 (6) (2017) 066039.
- [25] K. Toi, et al., [Effects of toroidally-distributed-divertor biasing on scrape-off-layer \(sol\) current drive, divertor particle flux and fast electron confinement in the quest spherical tokamak](#), Nuclear Fusion 63 (10) (2023) 106018.
- [26] B. Cui, et al., [2d pic modeling of the helical scrape-off layer current driven by hybrid divertor biased targets in tokamak plasmas](#), Nuclear Fusion 64 (12) (2024) 126027.
- [27] J. Degrave, et al., [Magnetic control of tokamak plasmas through deep reinforcement learning](#), Nature 602 (7897) (2022) 414–419.
- [28] B. Zhu, et al., [Data-driven model for divertor plasma detachment prediction](#), Journal of Plasma Physics 88 (5) (2022) 89580504.
- [29] B. Dudson, et al., [Hermes-3: Multi-component plasma simulations with bout++](#), Computer Physics Communications 296 (2024) 108991.
- [30] G. Holt, et al., [Tokamak divertor plasma emulation with machine learning](#), Nuclear Fusion 64 (8) (2024) 086009.
- [31] Y. Poels, et al., [Fast dynamic 1d simulation of divertor plasmas with neural pde surrogates](#), Nuclear Fusion 63 (12) (2023) 126012.